VSP

Journal of Adhesion Science and Technology 24 (2010) 2079–2104

Journal of ADHESION SCIENCE and TECHNOLOGY
brill.nl/jast

Cell Adhesion Monitoring Using Substrate-Integrated Sensors

Andreas Janshoff [a], **Angelika Kunze** [a], **Stefanie Michaelis** [b], **Vanessa Heitmann** [b], **Bjoern Reiss** [b] **and Joachim Wegener** [b,*]

[a] Institut für Physikalische Chemie, Universitaet Goettingen, Tammannstr. 6, 37077 Goettingen, Germany

[b] Institut fuer Analytische Chemie, Chemo- & Biosensorik, Universitaet Regensburg, Universitaetsstr. 31, 93053 Regensburg, Germany

Abstract

Adhesion of mammalian cells to *in vitro* surfaces is an area of active research and it attracts considerable interest from various scientific disciplines, most notably from medical technology and biotechnology. One important issue in the context of cell–surface adhesion is the time course of attachment and spreading upon surfaces that are decorated with proteins to make them cytocompatible. This article reviews two emerging non-microscopic techniques capable of monitoring the adhesion process label-free and in real-time. Both approaches, electric cell–substrate impedance sensing (ECIS) and the quartz crystal microbalance (QCM), are based on substrate-integrated transducers that transduce cellular adhesion into an electrical signal. A short introduction of both techniques is followed by a set of examples that illustrate the performance of these sensors, their individual merits and limitations. In order to analyze the integral and complex signals of both sensors in contact with mammalian cells in more detail, we also studied their individual readouts during the adsorption of liposomes with well-defined structure and chemical composition.

Keywords

Electric cell–substrate impedance sensing (ECIS), quartz crystal microbalance (QCM), cell adhesion, cell spreading, cell-matrix interactions, cell–surface junction, liposome adsorption

1. Adhesion of Animal Cells to *in Vitro* Surfaces: Why Bother?

The interactions of living cells with *in vitro* surfaces play a key role in a growing range of biomedical and biotechnological applications that aim to anchor cells tightly to inorganic substrates *in* or *ex vivo*. But also the opposite situation is sometimes of importance when all kinds of efforts are undertaken to keep cells from adhering upon such surfaces. In both cases suitable sensors and devices are required to study the adhesion of cells to such substrates. In this context, the term *cell*

* To whom correspondence should be addressed. Tel.: +941-943-4546; Fax: +941-943-4491; e-mail: Joachim.Wegener@chemie.uni-regensburg.de

 DOI:10.1163/016942410X507939

generally encompasses both eukaryotic as well as prokaryotic organisms but this article will only deal with sensors to detect the adhesion of *animal or human cells* to *in vitro* surfaces. Throughout this manuscript we will use the terms biomaterial surface, material surface, technical surface or *in vitro* surface as synonyms for the surfaces of man-made materials that are used for implants or other devices that are brought into contact with living mammalian cells.

Medical technology is one of the most important areas in which the interactions between animal or even human cells and biomaterial surfaces is of critical importance, in particular when it comes to designing endoprostheses or implants. When an implant is placed inside a living organism in order to fulfill structural or functional tasks, its biocompatibility is an unconditional prerequisite [1]. Very often the term biocompatibility means integration of the device into the target tissue and settling of the tissue-specific cells on its surface without creating a foreign-body response. But in many cases this is just a minimum requirement and the proper functionality of the implant requires strong and mechanically stable adhesion of the cells to the surface. Well-known examples of such implants are polymer tubes that are used to create bypasses, for instance, around plugged coronary arteries. In order to make the polymer surface blood compatible, endothelial cells (i.e. the cells that line the native blood vessels *in vivo*) are grown on the inner surface of the tubing, providing a vascular surface similar to the one inside the native vessels [2, 3]. Since the endothelial cells are exposed to significant shear forces by the circulating blood stream, their adhesion to the inner wall of the tubing is crucial and has to withstand considerable mechanical stress. In the exciting development of neuroprostheses, the requirements with respect to the cell-material contact zone are even more challenging as a real functional interfacing of the cells with electrodes or semiconductor devices is required. Besides mechanical stability, the cell–surface junction has to allow for a sensitive bi-directional transfer of electrical signals between the cells and the *in vitro* transducer [4, 5]. Animal cells interfaced with semiconductor devices have nowadays become emerging tools for drug and cytotoxicity screening *in vitro* [6].

Another less medical but more biotechnological example that demonstrates the importance of tailor-made cell–substrate adhesion and proper sensing devices to study it is the design of bioreactors in which animal cells are used for the large-scale production of proteins or fine chemicals. To improve the space–time-yield of such processes, the producer cells are frequently grown on the surface of micro-carrier beads that provides a higher ratio of available growth surface to reactor volume. However, the cells have to withstand the shear forces associated with the flow-through of medium that provides oxygen and nutrients. Thus, the anchorage of the cells to the surface of the carrier beads is decisive for the productivity of the bioreactor [7] and needs to be studied to find the optimum process conditions.

The interactions of cells with *in vitro* surfaces are considered and studied in the above-mentioned fields of applied science where they are important for the functionality of a certain process or device. Whenever cells are cultured *in vitro* they

will encounter *in vitro* surfaces, attach to them *via* cell–surface interactions and may even require substrate anchorage for their survival. It is well known that so-called *anchorage-dependent cells* will die if they cannot find a suitable place to adhere to and express proper cell–surface interactions [7]. But the surfaces have to fulfill certain conditions in order to be accepted or tolerated as an adhesion site for the cell. It is important to recognize that in many cell types certain signal transduction cascades are triggered upon attachment and spreading on a particular surface and this, in turn, may alter their differentiation or functional properties. Thus, the appropriate *in vitro* handling of stem cells, that typically show an undifferentiated phenotype but may follow certain wanted or unwanted differentiation pathways if they encounter *in vitro* surfaces, requires detailed knowledge about the molecular architecture of their cell–surface adhesion sites [8].

All the above-mentioned examples demonstrate that cell–surface adhesion plays a role in many fields of applied and fundamental research. A major problem that might have hampered research progress is the fact that the contact zone between cell and surface is not easy to access experimentally since it is buried between the cell body on the one side and the substratum on the other. Modern and extremely powerful techniques like scanning force microscopy (SFM), scanning electron microscopy (SEM) or other scanning probe techniques can provide very detailed images of the upper cell surface but they do not have access to the interface between lower cell membrane and the substratum to which the cell is attached. Of course, the cell bodies can be removed in order to study the molecular composition on the surface but it is an inherent problem whether the removal of the cell body has changed the interface with respect to its chemical and structural composition. To overcome this limitation, specialized analytical techniques and sensors have been developed that are tailor-made to study the contact area between cells and biomaterial surfaces. In this article we will focus on two emerging techniques that are based on physical sensors that are an integral part of the growth surface and that have proven to be very versatile and sensitive to monitor cell adhesion.

2. Key Events during Adhesion of Animal Cells to *in Vitro* Surfaces

Attachment and spreading of cells on *in vitro* surfaces is an enormously complex process. It requires the presence of adhesion-promoting proteins that are pre-immobilized on the surface of interest providing binding sites for specific receptor molecules expressed on the cell surface. Animal cells are unable to adhere to bare surfaces that are not decorated with pre-adsorbed proteins. The adhesion-promoting proteins are either pre-deposited from a protein solution before cells are seeded or the adhesive molecules are synthesized and secreted by the cells themselves. In particular, the latter option is often overlooked when cells attach and spread on an *in vitro* surface in a protein-free environment. Given this critical dependence of cell adhesion on the presence of adhesion-promoting proteins on the surface, it is obvious that the suitability of the surface to allow for protein adsorption is a pre-

requisite for being *cell compatible*. Here, wettability and surface topography are generally considered as the most relevant surface parameters for protein adsorption [9]. Neglecting the differences observed for individual proteins, there seems to be a general trend that the amount of protein that adsorbs on a given surface is higher when the surface is hydrophobic. However, when encountering a hydrophobic surface the protein may experience unfolding accompanied by a loss of its adhesive properties. On a hydrophilic surface the amount of protein that adsorbs is generally smaller but the protein retains its biological folding and will be recognized by the cell–surface receptors. Thus, this very general concept implies that *in vitro* surfaces should be hydrophilic in nature in order to be well suited for cell adhesion. Protein adsorption on a suitable surface generally occurs instantaneously. Spatz and collaborators recently demonstrated that the cells need suitable binding sites on the surface within certain distances in order to nucleate the formation of stable adhesion sites. Distances between individual surface binding sites of more than 73 nm do not allow for stable cell adhesion, while distances of less than 58 nm provided mechanically stable focal adhesion sites [10]. *Focal adhesion* is a term used in cell biology to describe the accumulation of individual, molecular cell-to-surface interactions in certain spots or foci on the surface which are particularly stable.

When a cell suspension is allowed to settle on an *in vitro* surface that is decorated with adhesive proteins, the initially suspended and mostly spherical cells first have to get close to the surface by sedimentation. The time necessary for a cell to reach the surface can be calculated from Stoke's law. For a spherical cell of 10 μm radius the sedimentation velocity can be estimated to be approximately 1 mm/min (assuming a cell density of 1.05 g/cm^3). Close to the surface, however, sedimentation becomes slower as the drainage of fluid between cell body and the flat surface requires additional time. Formation of first adhesive contacts between an almost spherical cell and the *in vitro* surface is generally considered as *attachment* or *adhesion*. Soon after first molecular contacts between substrate-immobilized proteins and the corresponding receptors on the cell surface have been established, the cells start to actively spread out accompanied by an extension of their contact area as illustrated in Fig. 1. Spreading out on the growth surface and areal extension of the cell-to-surface junction requires overcompensation of the cortical tension of the plasma membrane and the formation of new cell–surface contact sites along the periphery of the advancing cell body. The latter is a complex competition between specific cell–surface receptors and non-specific electrostatic interactions on the one hand with steric repulsion due to the necessary compression of extracellular material by the anchored cell body on the other [11]. It has been shown recently that the rate of cell spreading, s, is directly proportional to the ratio of energy necessary for cell adhesion E_{adh} and the cortical tension of the membrane σ_{Mem} [12]:

$$s \propto E_{\mathrm{adh}}/\sigma_{\mathrm{Mem}}. \tag{1}$$

Thus, reliable measurements of spreading kinetics for a given cell type but different biomaterial surfaces will provide the individual adhesion energies E_{adh} on a relative

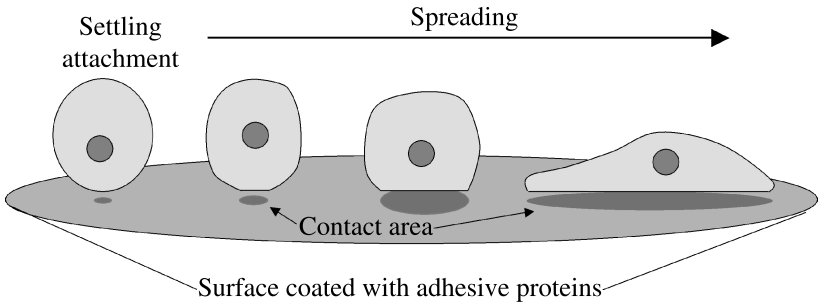

Figure 1. Changes in the three-dimensional shape of a mammalian cell during spreading on a cytocompatible culture substrate. The contact area between cell and surface increases continuously forming the cell-material interface.

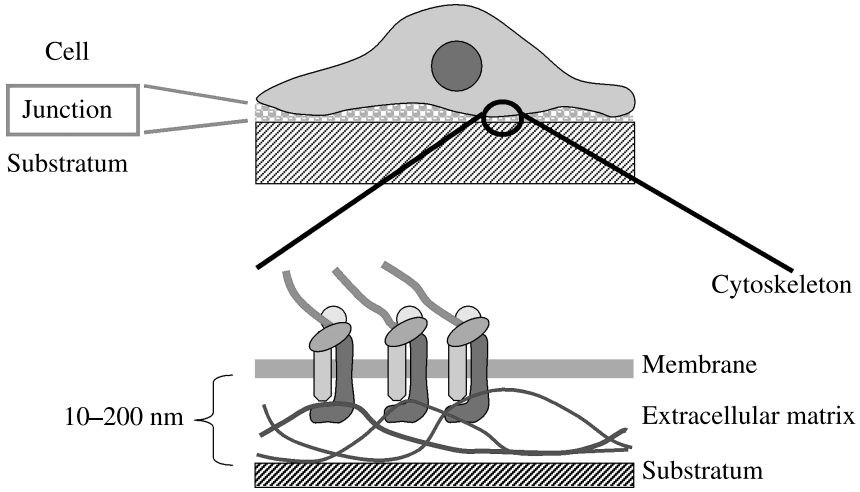

Figure 2. Schematic of the cell-material interface. Anchorage is provided by cell–surface receptors that bind specifically to components of the extracellular matrix on the substrate surface and are linked to the cytoskeleton on the intracellular side.

scale if one assumes that the cortical tension of the membrane is not affected by the nature of the surface, which is a reasonable assumption.

The geometrical distance between the substrate-facing cell membrane and the material's surface, after the cell has completely attached and spread, is a matter of debate. Figure 2 illustrates the situation at the cell–surface junction underneath a spread animal cell. Some authors report that in areas of closest adhesion between membrane and surface, so called *focal contacts,* the membrane gets as close as 5 nm to the surface [13]. Others report distances of up to 30 nm in these special regions. Areas in which the membrane is free of cell–surface receptors and, thus, is not involved in substrate adhesion can be as far as 200 nm away from the surface. However, in contrast to textbook presentations, Iwanaga *et al.* [14] did not find any correlation between the sites of *focal contacts* and sites of closest apposi-

tion of cell membrane and substrate. The *average* cell–substrate separation distance (averaged along the entire contact area) is generally reported to be between 25 and 200 nm, depending on the cell type and the coating of the substratum. The physical and chemical properties inside the cleft between cell and substrate are just on the verge of being characterized. It is well established nowadays that the narrow channel contains at least proteins and carbohydrates — which are the most prominent constituents of the extracellular material in almost any soft tissue — as well as water and salts. Very recent studies report that the specific conductivity within this small channel is indistinguishable from the bulk fluid that the cells are bathed in [15]. However, when vesicles or erythrocyte ghosts were attached to a surface, it was found that the conductivity in the remaining cleft was considerably reduced [16]. The reason for this change in ion mobility beneath the cells remains to be resolved.

3. ECIS and QCM: Two Interfacial Sensors to Monitor the Dynamics of Cell Adhesion

The number of experimental techniques capable of probing the contact area between adherent cells and their growth support is rather limited. All these techniques have in common that they were designed for one of the following objectives (i) to image the contact area between cells and substrate, (ii) to measure the distance between basal (i.e., substrate-facing) plasma membrane and surface, or (iii) to monitor changes in cell adhesion as a function of time. It is beyond the scope of this review to provide a comprehensive survey about all these available methods and to list their individual performances and limitations. The interested reader is referred to an article by one of us [17] and the references therein.

In this article, however, we focus on two unrelated, non-imaging techniques that are both label-free, non-invasive and capable of providing the dynamic aspect of cell adhesion in real-time. In the literature they are referred to as *Electric Cell-Substrate Impedance Sensing* (ECIS) and the *Quartz Crystal Microbalance* (QCM) techniques. In both cases the cells are allowed to adhere directly to the surface of the sensor and the accompanying sensor response is quantified by means of non-invasive electrical measurements. Compared to invasive ultra-structural or label-dependent techniques, the common strength of both approaches is to provide a dynamic time-resolved readout that allows to resolve even subtle details of the adhesion kinetics. In the following sections both approaches will be introduced briefly before their performance with respect to monitoring cell adhesion is discussed and compared.

3.1. A Brief Introduction to the ECIS Sensor Device

The idea of electric cell–substrate impedance sensing (ECIS) was introduced by Ivar Giaever and Charles R. Keese, who were the first to grow mammalian cells directly on the surface of gold-film electrodes and to record and analyze the corresponding changes in the electrode's electrical impedance [18, 19]. In the meantime

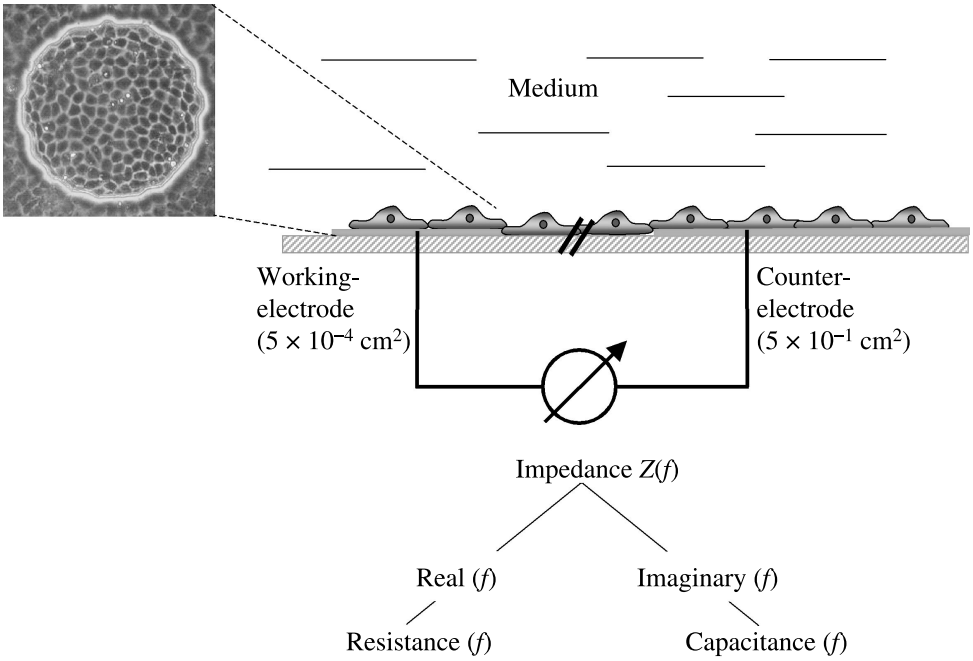

Figure 3. The principal of electric cell–substrate impedance sensing (ECIS). The cells under study are grown on the surface of gold-film electrodes deposited on the bottom of a cell culture vessel. The impedance measurement is dominated by the electrical properties of the smaller working electrode. The area of the working electrode is delineated by a circular opening ($d = 250$ μm) in a photoresist overlayer that insulates the rest of the deposited gold from the bulk electrolyte. Note that the size of the electrode in the magnified presentation is not drawn to scale with respect to cell size.

several other groups have followed this basic concept but used other electrode materials, geometries, or different recording setups [20–22].

The basic principle of the ECIS technique is sketched in Fig. 3. Two coplanar gold-film electrodes are deposited on the bottom of a polymer dish and the cells are allowed to settle, adhere and spread on these surfaces under ordinary cell culture conditions. The electrical connection between the two electrodes is provided by the culture medium, a buffered physiological salt solution of app. 15 ms/cm conductivity that contains all nutrients and growth factors that the cells require. The two electrodes differ with respect to their surface areas. By making the counter electrode 1000 times larger than the small working electrode, the impedance of the latter dominates the read-out of the entire circuit. Thus, the observed changes in electrical impedance can be clearly assigned to changes that occur at the small working electrode with negligible contributions due to the presence of cell bodies on the counter electrode or the electrical wiring of the setup. The size of the working electrode is one of the most critical parameters when the sensitivity of the measurement is considered [23]. For bigger working electrodes it becomes increasingly difficult to record cell-related changes in impedance as the resistance of the bulk electrolyte

gradually masks the impedance of the cell-covered electrode. Most data available in literature have been recorded with circular electrodes of 250 μm diameter.

In ECIS, impedance data are usually recorded over a frequency range between 1–10^6 Hz. In terms of information content this broad frequency range can be subdivided into two regimes:

(a) For the major fraction of this frequency band (<10 kHz for working electrodes with 250 μm diameter, as used here) the cells behave essentially like insulating particles forcing the current to flow around the cell body on paracellular pathways. Current leaving a cell-covered electrode has to flow through the confined and narrow channels between the ventral plasma membrane and the electrode surface before it can escape through the paracellular shunt between adjacent cells into the bulk phase (Fig. 2). Since the current has to bypass the cell bodies it picks up impedance contributions from the cell–substrate adhesion zone as well as from the contact area between neighboring cells. Readings of the total impedance are thus sensitive to changes in cell–cell and cell–substrate contacts or cell shape in general. Recording the impedance at several frequencies in this regime together with theoretical modeling allows to assign the individual impedance contributions either to the cell–substrate or the cell–cell contact sites. Details of the modeling are not addressed here but the interested reader is referred to [24].

(b) For monitoring cell adhesion, high frequency readings (>10 kHz for working electrodes with 250 μm diameter, as used here) of the complex impedance are particularly useful [25]. At these frequencies, the current can capacitively couple through the cells passing the ventral and the dorsal membranes in the form of a displacement current. At these frequencies it does not flow around the cells to a significant extent.

For cell adhesion studies it is worthwhile to look deeper into measurements of the complex impedance. The impedance, in general, consists of a real (resistance, R_{total}) and an imaginary part (reactance, X_{total}). The former contains all resistive contributions of the system, whereas the latter includes all capacitive contributions. From equation (2)

$$C_{\text{total}} = 1/(2 \cdot \pi \cdot f \cdot X_{\text{total}}) \tag{2}$$

it is possible to calculate the equivalent capacitance of the whole system C_{total} which is the most useful parameter in terms of dynamic cell adhesion monitoring as will be detailed below. In equation (2) f denotes the AC frequency.

For a cell-free electrode the measured capacitance C_{total} at a given frequency is equal to the electrode capacitance:

$$C_{\text{total}} = C_{\text{electrode}}. \tag{3}$$

For a *cell-covered* electrode and frequencies above 10 kHz, C_{total} is comprised of the capacitance of the electrode (as before) and the capacitances of the two membranes (ventral and dorsal) which are now arranged in series to

$C_{\text{electrode}}$. According to Kirchhoff's laws about electrical circuitry the measured capacitance C_{total} for an electrode entirely covered with cells is

$$1/C_{\text{total}} = 1/C_{\text{cell-covered}} = 1/C_{\text{electrode}} + 1/C_{\text{membrane1}} + 1/C_{\text{membrane2}}. \quad (4)$$

During cell attachment and spreading on the electrode surface, the fraction of the electrode that is covered with cells — or the plasma membranes of the cells — increases with time. As the capacitance scales with the area the following relationship applies for all intermediate situations with a partly covered electrode:

$$C_{\text{total}} = (1 - x_{\text{coverage}}) \cdot C_{\text{cell-free}} + x_{\text{coverage}} \cdot C_{\text{cell-covered}} \quad (5)$$

with x_{coverage} as the ratio of cell-covered and total electrode area ($0 \leqslant x_{\text{coverage}} \leqslant 1$). Correspondingly, the total capacitance C_{total} changes linearly with the fraction of the electrode that is covered by a planar layer of two cell membranes and thus with the fraction of the electrode covered by spread cells.

In summary, measuring the total capacitance of the system is the most direct approach to monitor the coverage of the electrode surface as a function of time. As the capacitance is easy to record at this frequency, measurements of C_{total} provide an easy and accurate determination of the spreading kinetics which can be used to determine the adhesion energy as stated above. However, this very convenient linear relationship only applies as long as the frequency of the AC current is high enough such that all current traversing the cell layer takes the transcellular route across the plasma membranes.

It should be noted at this point that other authors [20] chose to interpret the measured impedance by using an equivalent circuit of an overall resistance (R_{p}) in parallel to an overall capacitance (C_{p}). Plotting this parallel capacitance C_{p} as a function of time is, however, not an equivalent way of monitoring cell spreading as the parallel capacitance responds in a more complicated way to electrode surface coverage at most frequencies.

3.1.1. ECIS-Based Cell Adhesion Monitoring

The considerations discussed in the preceding section indicated that measuring the total capacitance of the ECIS electrode C_{total} at a sampling frequency >10 kHz should provide a sensitive measure to follow the spreading of animal cells in real time. We have studied the suitability of C_{total} experimentally by performing different sets of experiments that all required a very detailed recording of spreading kinetics. As sampling frequency we have arbitrarily chosen 40 kHz but any frequency above the frequency threshold of 10 kHz works similarly well. From an experimental viewpoint it is important to stress that we used rather high cell densities in a more or less mono-disperse cell suspension for inoculation ($5 \times 10^5/\text{cm}^2$) to ensure that the recorded signal only reported on cell attachment and spreading without any contributions from cell proliferation. The number of cells seeded into the electrode containing wells was sufficient to form a confluent monolayer on the

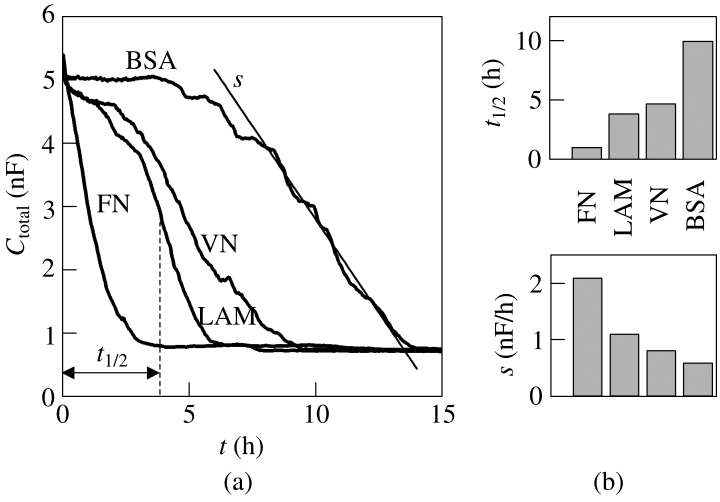

Figure 4. (a) Time courses of the capacitance C_{total} measured at a sampling frequency of 40 kHz when MDCK cells were seeded into ECIS arrays whose electrodes had been coated with fibronectin (FN), laminin (LAM), vitronectin (VN) or bovine serum albumin (BSA) in 100 µg/ml concentrations, respectively. The slope of each curve s between $C_{\text{total}} = 4$ nF and $C_{\text{total}} = 2$ nF — equivalent to the apparent rate of spreading — was extracted by linear regression as shown for the BSA-coated electrode. (b) Half-times $t_{1/2}$ and apparent spreading rates s as determined from the data shown in (a) [25].

surface without any need for cell division. Moreover, this approach ensured a homogeneous coverage of the well bottom so that no normalization for local cell density was necessary.

Figure 4(a) shows the time course of the electrode capacitance C_{total} at a sampling frequency of 40 kHz when equal numbers of suspended MDCK-II cells (Madin Darby canine kidney) attached and spread on four ECIS electrodes that had been coated with different protein layers prior to cell seeding [25]. Two parameters have been extracted to quantitatively compare the dynamics of cell spreading. The parameter $t_{1/2}$ denotes the time required for half-maximum spreading of the cells; whereas the parameter s stands for the apparent spreading rate (Fig. 4(b)), which is deduced from the slope of the curve at $t = t_{1/2}$ (Fig. 4(a)). It is noteworthy that according to equation (1), the spreading rate s is directly proportional to the adhesion energy E_{adh} of the cells for a particular surface.

The four traces in Fig. 4(a) show that MDCK cells apparently attach and spread much faster on surfaces coated with fibronectin (FN) compared to all other proteins used in this experiment. According to the parameters $t_{1/2}$ and s, the kinetics for cell adhesion to vitronectin (VN) and laminin (LAM) decorated electrodes is rather similar. For bovine serum albumin (BSA) coating it requires more than five hours before the cells even start to spread out significantly. The half-times $t_{1/2}$ of LAM, VN and BSA coatings clearly mirror this huge difference in spreading dynamics. Consistent with these findings BSA is considered to be a non-adhesive protein. The

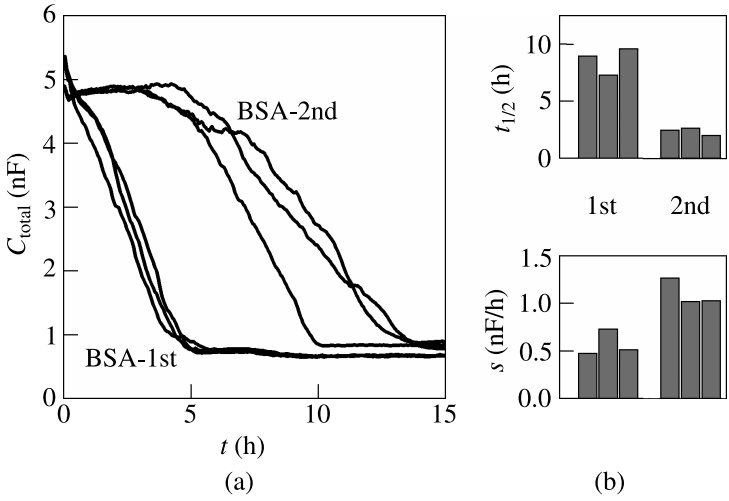

Figure 5. (a) Time course of the capacitance C_{total} measured at a sampling frequency of 40 kHz when MDCK cells were seeded into ECIS arrays whose electrodes had been coated with 100 µg/ml BSA (BSA-1st). After 24 h these cells were gently removed from the surface and a fresh cell suspension was seeded on the same electrodes (BSA-2nd). The figure shows triplicates for each condition. Serum-free medium was used in both cases. The figure shows (b) half-times $t_{1/2}$ and apparent spreading rates s as determined from the data shown in (a) [25].

apparent spreading rate s for BSA, however, is surprisingly close to the values for LAM and VN indicating at first sight that the cells eventually spread on this protein layer with similar kinetics — or in other words and according to equation (1) that the adhesion energy is apparently similar for these three coatings.

The experiment shown in Fig. 5 explains these data from a different viewpoint [25]. Here, equal numbers of MDCK cells were inoculated on three electrodes that were all pre-coated with BSA under identical conditions (1st inoculation, Fig. 5(a), BSA-1st). After 20 hours the cells were gently removed from the surface and a fresh cell suspension was inoculated on the identical electrodes that had been used in the preceding experiment (2nd inoculation, Fig. 5(a), BSA-2nd). Now the cells attach and spread much faster and the kinetic parameters of the second inoculation are similar to those that had been determined for a LAM coating (see Fig. 4). The explanation for these observations is that the cells that had been first inoculated on the BSA coated electrodes had synthesized adhesive proteins and secreted them on the electrode surface. Since the biosynthesis of these proteins requires time, it took roughly five hours before the cells started to spread on their self-made extracellular matrix. When the adherent cells were gently removed from the surface, their adhesive proteins were left behind and the cells that had been inoculated afterwards found a layer of adhesive proteins already on the surface. The spreading characteristics of the second inoculation indicate that the initially seeded cells might have secreted LAM onto the surface. Consistent with this experiment, it has been reported that MDCK cells synthesize and secrete LAM [26].

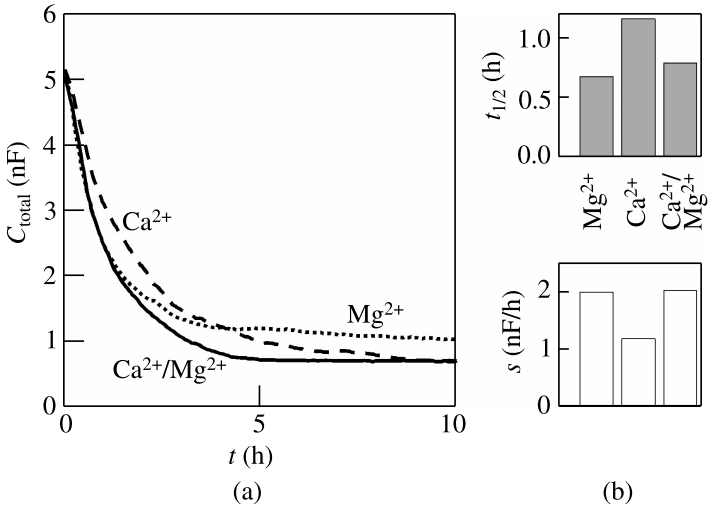

Figure 6. (a) Time course of the capacitance C_{total} measured at a sampling frequency of 40 kHz when MDCK cells were seeded into ECIS arrays whose electrodes had been coated with 100 µg/ml fibronectin. The cell suspension was prepared in Earles' balanced salt solution with Ca^{2+} and Mg^{2+} (solid); Mg^{2+} only (dotted), or Ca^{2+} (dashed) only. (b) Half-times $t_{1/2}$ and apparent spreading rates s as determined from the data shown in (a) [25].

The outstanding sensitivity of capacitance readings to monitor the substrate-anchorage of living cells could be nicely demonstrated in experiments, in which adhesion of MDCK cells to FN coated electrodes was studied in the presence of physiological concentrations of either Ca^{2+}, or Mg^{2+} or both. Binding capabilities of those cell–surface receptors that are responsible for FN binding depend on the presence of divalent cations. Some integrins show a selectivity for Ca^{2+} over Mg^{2+} or *vice versa* [27]. Figure 6 shows the time course of the electrode capacitance at 40 kHz when initially suspended MDCK cells attach and spread onto FN coated electrodes in the presence of either Ca^{2+}, Mg^{2+} or both. Apparently, MDCK cells attach and spread slightly faster onto a FN coating when Mg^{2+} is present in the culture fluid, either alone or in co-presence of Ca^{2+}. When Ca^{2+} is the only available divalent cation, spreading kinetics is slightly retarded. It is also apparent that the electrode capacitance drops to smaller values when Ca^{2+} is present in the fluid either alone or in co-presence of Mg^{2+} indicating that the cell morphology is slightly different in the presence or absence of Ca^{2+}.

3.1.2. Latex Spheres and Giant Liposomes as Simple Model Systems for Living Cells

In order to validate the performance of the ECIS device with well-defined chemical model systems we chose to study with exactly the same experimental setup the adhesion of (i) latex spheres (particle surface not chemically modified) of 3 µm diameter and (ii) liposomes (vesicles) that were prepared to have roughly cellular dimensions [28]. The latex spheres served as a model for hard particles that will

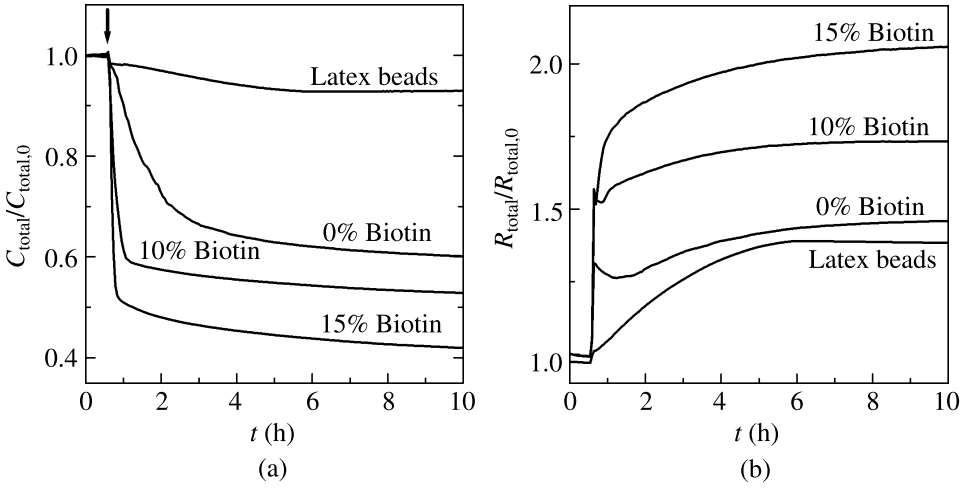

Figure 7. Time course of the capacitance C_{total} (a) and resistance R_{total} (b) measured at 40 kHz during adsorption of vesicles on the avidin-coated electrodes. Vesicles contain different concentrations of biotinylated lipid, 0%, 5%, 15%. For comparison, the time dependent adsorption of latex beads on uncoated electrodes is included. For better comparison both quantities are normalized to the starting values at time zero [28].

not spread but attach in spherical form. The giant liposomes were used to simulate cell spreading. In order to induce liposome attachment and spreading the electrodes were coated with the biotin-binding protein avidin while the liposome shell was doped with the corresponding biotin-labeled lipids. Comparing the liposome system with a cellular system, the biotinylated lipids represent the cell–surface receptors while the avidin coating of the electrodes simulates the deposition of adhesion-promoting proteins.

Figure 7 compares the time course of the measured capacitance C_{total} when giant vesicles doped with different mole fractions of biotinylated lipids as well as latex beads of 3 μm diameter were added to the bulk solution and were allowed to settle on an avidin-coated electrode [28]. The capacitance values have been normalized to the starting value at time zero. It is evident that the liposomes induce a considerably larger capacitance reduction compared to the latex beads. The reason for this is that the latex spheres behave like hard particles with only a very limited contact area with the electrode surface. Thus, the current flows exclusively around the particles even at 40 kHz. The more flexible giant liposomes, however, spread out to a certain degree on the electrode surface, forming an extended area of close contact with the electrode. The biotin-doped liposomes show faster adsorption kinetics compared to the biotin-free controls indicating that the specific biotin–avidin interaction affects the kinetics of cell adhesion and, thus, the adhesion energy E_{adh}. But not only the kinetics is different, we also observed significant differences in the final capacitance which ranged between 0.6 for the normalized capacitance for the undoped vesicles to 0.4 for the highest biotin doping of 15% (w/w). However, we

know from preceding SFM studies that the liposomes show a stronger spreading and flattening on avidin-coated surfaces with increasing biotin content [29]. The contact area with the protein-coated substrate grows with increasing biotin content giving rise to a more pronounced capacitance decrease with the same number of vesicles on the surface. Thus, the magnitude of capacitance reduction is assumed to reflect the more sustained spreading of the liposomes with increasing biotin content. Figure 7(b) shows the time-dependent increase of the total resistance obtained at a sensing frequency of 40 kHz for the same model systems. Due to the presence of the dielectric structures close to the electrode surface the resistive portion of the impedance is increased as well. Moreover, with higher biotin concentration the resistance increase is more pronounced but rather low for the hard latex spheres. The resistance readout is, however, more difficult to interpret in terms of surface coverage since the initial jump in resistance is due to the unavoidable change in electrolyte composition that is associated with vesicle addition to the bathing fluid. Moreover, there is no simple correlation between surface coverage and magnitude of resistance increase since the latter is also affected by the constriction of current flow between adjacent liposomes.

Taken together, ECIS is one of the emerging techniques that can be applied in various modes to monitor the formation and modulation of cell–substrate interactions with high time-resolution compared to the time scale of the biological phenomenon under study. ECIS is not confined to electrodes made from gold but can also be applied to other conducting supports. Gold, however, is the best suited material due to its high electrical conductivity, chemical inertness and electrochemical characteristics. Unfortunately, the gold electrode cannot be coated with thin layers of other technical materials like, for instance, polymers without losing the capability for electrochemical measurements due to the presence of an insulating electrode coating. This limits the field of potential applications to electrode coatings that are conducting and do not interfere with the ECIS measurements.

3.2. A Brief Introduction to the QCM Technology

The second emerging technique to study the adhesion of cells to *in vitro* surfaces is the so-called *quartz crystal microbalance* (QCM) technique [30–32]. The QCM had already been well-known and established as an analytical tool to study adsorption phenomena at the solid–liquid interface when its potential to study cell–substrate adhesion was recognized. The approach is based on thin disks made from α-quartz that are sandwiched between two metal electrodes (Fig. 8). Due to the piezoelectric nature of α-quartz, any mechanical deformation of the crystal creates an electrical potential difference at the quartz surfaces and *vice versa*. Thus, mechanical oscillations of the crystal can be triggered, stabilized and recorded electrically. The mode of mechanical deformation (e.g., shear, torsion) in response to an electrical potential difference between the two surface electrodes depends on the crystallographic orientation by which the thin disk-shaped resonator has been cut out of a single crystal of α-quartz. For QCM purposes, only AT-cut resonators are used that

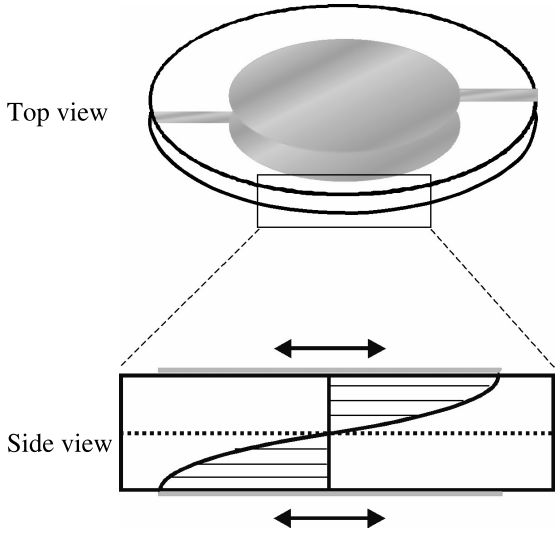

Figure 8. Top and side views on AT-cut thickness shear mode resonators as they are used in the QCM technique. The disk-shaped resonator is sandwiched between two gold-film electrodes that are used to drive the resonant oscillation and to read the resonance frequency. Under resonance conditions a standing acoustic wave is established between the crystal's surfaces that is sensitive to adsorption and desorption reactions occurring at the surface.

perform shear oscillations parallel to the surface with the maximum amplitude at the crystal faces (see Fig. 8). At resonance the mechanical shear displacement of the crystal responds very sensitively to the adsorption of a foreign material on the resonator surface. It was Sauerbrey who found already in 1961 [33] a linear correlation between the observed shift of the resonance frequency and the foreign mass that was deposited on the surface. Since frequency shifts of electrical oscillations can be measured very accurately, the device is capable of reporting the adsorption of sub-microgram quantities on the surface which gave it the name *quartz crystal microbalance*.

It was then recognized that the interactions of cells with the quartz surface also induced a shift in resonance frequency that was shown to be correlated with the degree of surface coverage [34–36]. Thus, time resolved measurements of the resonance frequency can be used to follow the attachment and spreading of cells on the quartz surface. As the fundamental resonance of the thickness shear mode (TSM) resonators that are used for QCM experiments is in the MHz regime, the time resolution of such measurements can be pushed down to milliseconds. Moreover, we and others have found that confluent monolayers of different cell types (i.e., 100% coverage) produce individual, cell-type specific shifts of the resonance frequency [37]. The structural reasons for these individual shifts in resonance frequency are not yet fully understood but may report on the individual molecular architecture of cell–substrate contacts, different adhesion mechanics, cell-type specific viscoelasticity, cell-type specific density of cell–substrate contacts per unit area or — and the

most relevant — cell-type specific micro-mechanics of the membrane that is facing the substrate.

In contrast to ECIS, it is a unique and important feature of the QCM technique that the measurement is still possible when the quartz resonator is first coated with a thin layer of any material to be tested for biocompatibility. These thin material layers can be of metallic, polymeric or ceramic nature. The only limitation is that the pre-adsorbed material layer is rigid in nature, of limited thickness (generally below a few micrometers) and does not produce significant acoustic losses. In particular, the applicability to a wide variety of materials — after they had been coated on shear wave resonators — renders the QCM technique a universal and versatile sensor for cell-material interactions.

Several experimental issues are noteworthy for QCM-based cell adhesion studies:

(a) Due to energy trapping, the quartz resonator is only sensitive to changes of the surface load in those areas of the resonator that are covered with electrodes. We typically use quartz resonators with a diameter of 14 mm but the centro-symmetric electrodes on either side of the crystal are only 6 mm in diameter. Thus, similar to the ECIS setup the sensitive area inside this "wired Petri dish" is just a fraction of the total area that is available for cell adhesion.

(b) Even within the area that is covered by electrodes, the local sensitivity of the resonator is not uniform but falls off with increasing distance from the electrode center. Whereas the sensitivity is maximal in the center of the electrode, it fades to zero at the electrode edges. This well-known fact is important to recognize when cell adhesion experiments are conducted as it requires very homogeneous, single cell suspensions at the beginning of the experiment. Otherwise the readout may show significant scatter as it depends a great deal on where the cells adhere to the sensor [38].

(c) The Sauerbrey relationship, as it was introduced above, does not apply when cells are studied by means of QCM measurements. The cell bodies do not behave like a rigid mass layer but much more like a viscoelastic body [39, 40]. Thus, it is not valid to translate the observed frequency shift to biomass simply using the Sauerbrey equation and the integral mass sensitivity of the device. Ignoring this fact and applying the Sauerbrey relation anyway leads to a significant underestimation of the cell mass by QCM measurements [41].

(d) The QCM is often — and in most cases correctly — considered as a mass sensing device. However, in addition to what is discussed in (c) it is also important to realize that the QCM is only sensitive to the first monolayer of cells in direct contact with the resonator surface. Additional cells settling down on the first monolayer without direct contact with the sensor surface are not registered. The method is essentially blind to changes occurring beyond the first cell monolayer unless there is an indirect response of the cells to these activities or the surface-attached cells form very thin extensions with only a few hundred nanometers in height. If the resonator is loaded with pure water at room temperature, the decay length of the mechani-

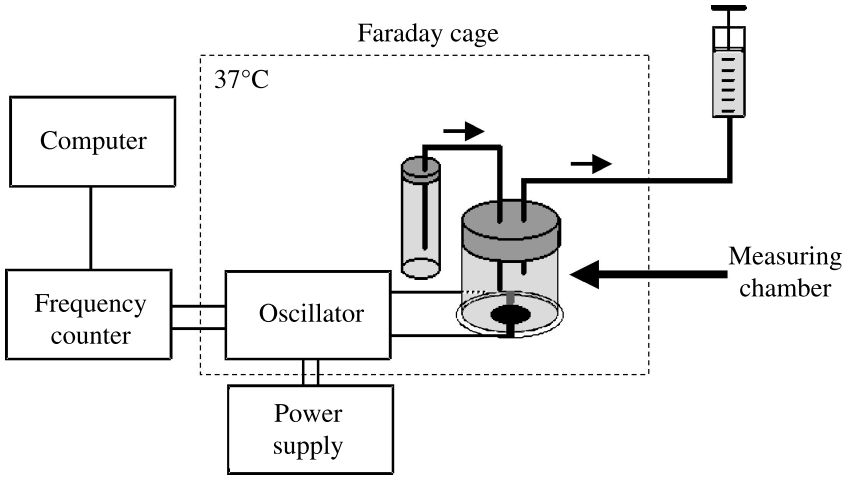

Figure 9. Experimental setup to monitor the time course of cell attachment and detachment by reading the resonance frequency of the quartz resonator that forms the bottom plate of the cell culture vessel. The measuring chamber is housed in a 37°C incubator.

cal shear wave amounts to 250 nm. This decay length is unknown for cell-covered resonators but we could show experimentally that the shear wave does not escape the cell bodies with considerable amplitude if the cells are several micrometers in height [42].

3.2.1. QCM-Based Cell Adhesion Monitoring

Figure 9 shows a schematic of the experimental setup that was used in our laboratory to measure the shift in resonance frequency during attachment and spreading of cells [37]. The quartz resonator with a fundamental resonance frequency of 5 MHz forms the bottom plate of a measuring chamber that holds approximately 0.5 ml of cell suspension. The oscillation at minimum impedance $Z_{\min}$ is stabilized by a feedback-control oscillator circuit[1] that is placed close to the crystal inside a temperature controlled Faraday cage (37°C). The oscillator circuit is driven by a 5 V power supply and the resonance frequency is determined by a commercially available frequency counter. The interested reader can find very different hardware approaches for QCM measurements in the literature that may even report two quantities: the resonance frequency and the quality factor of the oscillation which indicates viscous losses [43].

3.2.2. Time Course of Attachment and Spreading

Cells were seeded into the measuring chamber in a sterile flow hood. Immediately afterwards attachment and spreading of the cells was followed with time. Figure 10(a) compares the time-dependent shift in resonance frequency when increasing amounts of epithelial MDCK II cells are seeded into the chamber at time

[1] The oscillator circuit based on a Texas Instruments TTL chip was developed by A. Janshoff.

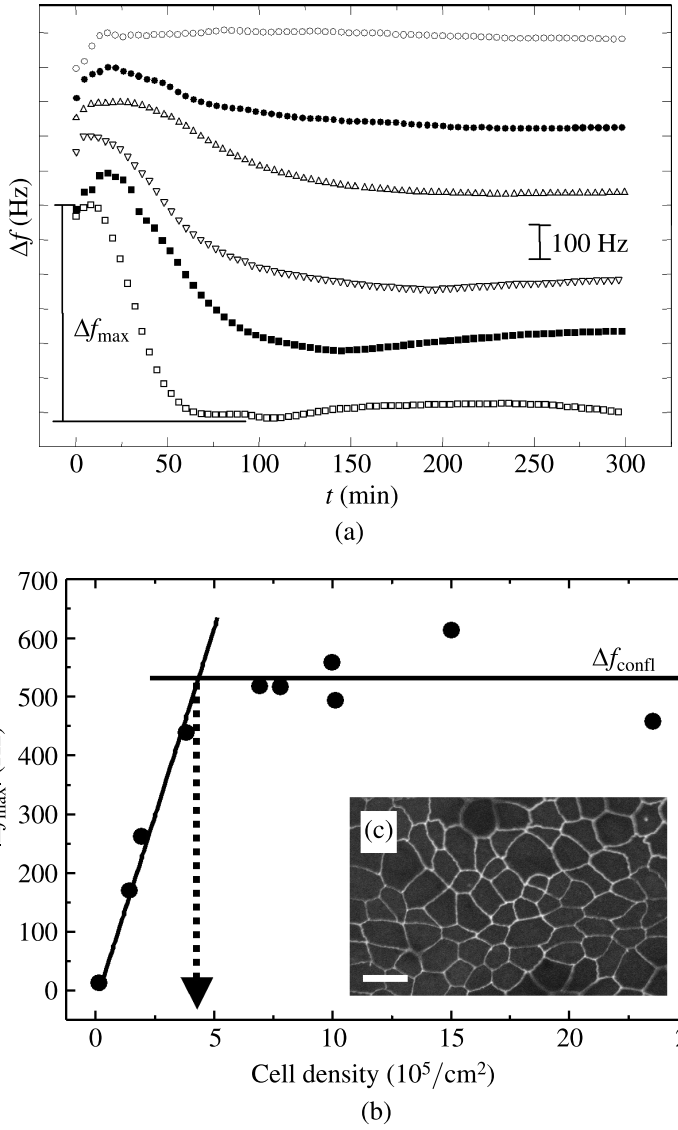

Figure 10. (a) Shift of the resonance frequency during attachment and spreading of initially suspended MDCK II cells. Each curve represents a different number of cells that were seeded at time zero. From the upper to the lower curve seeding densities were as follows (in cm^{-2}): open circles 0; filled circles 1.3×10^5; up triangles 1.8×10^5; down triangles 3.7×10^5; filled squares 7.7×10^5; open squares 1.5×10^6. Δf_{max} indicates the maximum frequency shift observed for a given seeding density. (b) Maximum frequency shift Δf_{max} as a function of the cell density that was seeded into the measuring chambers at time zero (see Fig. 10(a)). The intersection of the ascending and the horizontal lines corresponds to the number of cells on the surface (per unit area). Δf_{confl} denotes the frequency shift for a confluent cell monolayer. (c) Fluorescence micrograph of a confluent MDCK II cell layer after staining for a junctional protein exclusively localized at the cell border. The scale bar corresponds to 20 μm [36].

zero [36]. From the topmost to the bottommost curve in Fig. 10(a) the cell density in the measuring chamber was continuously increased from a cell-free control to a maximum of 1.5×10^6 cells/cm^2. Immediately after the start of the experiment there is a moderate increase of the resonance frequency by 50–100 Hz which is exclusively due to the warm-up of the medium inside the chamber to 37°C. After this transient maximum, the resonance frequency continuously decreases and it now reports the formation of cell–substrate adhesion sites and continuous progress in cell attachment and spreading. The time resolution of such measurements can be reduced well below one second so that even very subtle details of the cell adhesion kinetics can be monitored using QCM measurements. The slope of the curves is easily accessible and can be used to determine the adhesion energy for this cell type in contact with the biomaterial surface under study. The more cells are seeded the larger is the resulting shift in resonance frequency upon attachment and spreading.

When the maximum frequency shift $|\Delta f_{\max}|$ for an individual experiment as shown in Fig. 10(a) is plotted against the number of cells seeded into the measuring chamber at time zero, we obtain a saturation type relationship that is presented in Fig. 10(b) [36]. The data in Fig. 10(b) can be interpreted as follows: as long as the density of seeded cells is small enough that all cells reaching the surface can find an adhesion site, an increase in the maximum resonance frequency shift $|\Delta f_{\max}|$ is observed with increasing seeding density. This frequency shift is proportional to the fractional surface coverage as has been confirmed by others [34, 35]. However, when the number of seeded cells is increased further all adhesion sites on the surface are occupied and accordingly we do not find any further increase in $|\Delta f_{\max}|$. This observation convincingly underlines that the QCM device is primarily sensitive to phenomena that occur at the quartz surface but does not report on cells that are beyond the first cell monolayer [42]. Based on these data it is hard to imagine that biological activities that occur at the apical surface of an established cell layer can be observed by QCM unless the cells are very thin. It is, however, reported that exocytotic events in adherent cells can be monitored by the QCM approach [44].

If only those cells in direct contact with the resonator surface contribute to the overall signal, we should be able to determine the cell density on the surface from measurements as the one shown in Fig. 10(b). To do so, we have chosen a two-case approach: (i) for low seeding densities the relationship is approximated by a straight line with positive slope that indicates a linear correlation between frequency shift and surface coverage; (ii) beyond a certain cell density the experimental adhesion curve is modeled by a horizontal line indicating that surplus cells, that do not find adhesion sites on the substrate, do not contribute to the measured QCM response. Accordingly, the interception between these two straight lines should mark the actual cell density on the surface. For MDCK cells (strain II), that were used in these experiments, we found the interception to be located at a seeding density of $(4.3 \pm 0.5) \times 10^5$ cells/cm^2 (arrow in Fig. 10(b)). For validation we have also determined the cell density in an entirely confluent monolayer microscopically after the cell borders had been stained by immuno-cytochemistry. Figure 10(c) shows a

typical fluorescence micrograph that was used to determine the cell density. Images recorded by fluorescence microscopy revealed a cell density of $(5.5 \pm 0.3) \times 10^5$ cells/cm^2 on the surface which is slightly above the value extracted from QCM readings. However, microscopic experiments were conducted on cell monolayers that were allowed to grow to confluence for several days, while QCM experiments were limited to attachment and spreading within only 5 h. Since the cells tend to multiply to some degree even in a confluent monolayer before contact inhibition stops any further proliferation, it is not surprising to find somewhat higher cell densities in our microscopic control experiments. Repeating these kind of experiments with other cell types confirmed our conclusions. We found consistently that the number of cells on the surface was determined correctly from QCM readings. Interestingly, different cell types create individual shifts in resonance frequency when they adhere to the quartz surface. It is important to stress that these differences are not due to incomplete coverage of the quartz resonator but reflect individual differences in the contact mechanics or the mechanics of the substrate-facing membrane.

As already indicated above, *specific* molecular interactions of the receptor-ligand type as well as *non-specific* interactions contribute individually and at different times to the anchorage of cells to a given *in vitro* surface [11, 45, 46]. Compelling evidence has been collected that *specific* ligand–receptor interactions are more important for the final strength and the dynamic properties of the adhesion sites [45], whereas unspecific electrostatic or electrodynamic interactions are important during the first phase of the cell–surface encounter. Thus, the question arises whether the QCM response requires specific, receptor-mediated adhesion of the cells to the surface or the sole presence of the cell body close to the resonator surface. One strategy to answer this question is to block the specific interactions between cell–surface receptors and adhesive proteins on the substrate by adding short peptides to the culture fluid that compete with the adhesion-promoting proteins for the binding sites of the cell–surface receptors. When these soluble peptides are added to the cell suspension, they are expected to delay or entirely eliminate specific cellular interactions with substrate immobilized proteins.

In our experiments we used serum containing medium as culture fluid even though the chemical composition of serum is not precisely defined and may vary, to some degree, from batch to batch. Serum naturally contains the adhesive proteins vitronectin (VN) and fibronectin (FN), which adsorb instantaneously from solution to the surface. Both proteins, VN and FN, are recognized by cell–surface receptors *via* the same amino acid sequence Arg-Gly-Asp-Ser, or RGDS in one letter code. Thus, we studied the impact of soluble peptides with this amino acid sequence on the time course of cell attachment and spreading using the QCM approach. Figure 11 shows the outcome of two experiments in which either the penta-peptides Gly-Arg-Gly-Asp-Ser (GRGDS) or Ser-Asp-Gly-Arg-Gly (SDGRG) were added to the cell suspension in a concentration of 1 mM each [36]. The two penta-peptides GRGDS and SDGRG contain exactly the same amino acids but in reverse order. Thus, the two molecules carry the same charge density and would provide the same

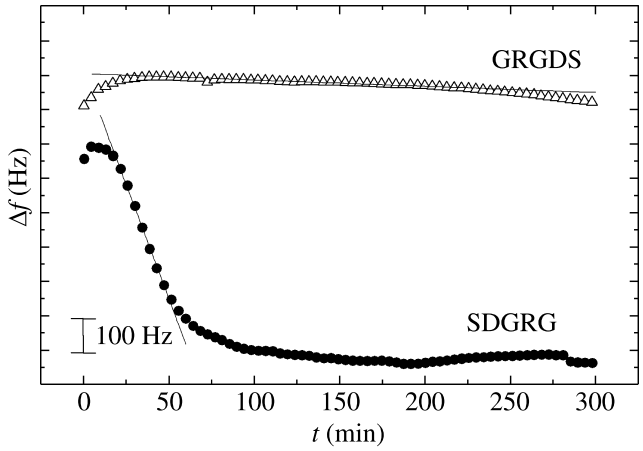

Figure 11. Time course of the resonance frequency during the attachment and spreading when similar numbers of MDCK II cells were seeded into the quartz dish in presence of the soluble peptides Gly-Arg-Gly-Asp-Ser (GRGDS) or Ser-Asp-Gly-Arg-Gly (SDGRG). The concentration of each peptide was 1 mM and the cell density was adjusted to 8×10^5 cm^{-2} [36].

perturbation to unspecific interactions — if at all. However, due to the reversal of the amino acid sequence only GRGDS has the correct sequence to interact specifically with the cell–surface receptors whereas SDGRG does not. The time course of the resonance frequency $\Delta f(t)$ as presented in Fig. 11 clearly demonstrates that in the presence of 1 mM GRGDS the resonance frequency does not indicate any cell adhesion to the resonator surface. In contrast, when SDGRG is added to the culture fluid, there is no difference compared to experiments in which no peptide is present at all (see Fig. 10(a)). Thus, when specific interactions between cell–surface receptors and substrate immobilized proteins are not allowed to form, we do not observe any measurable impact on QCM readings. The measurements clearly show that loose attachment of the cell bodies to the substrate does not produce any significant acoustic load and, moreover, that cells which are not capable of forming specific molecular interactions with substrate-immobilized proteins cannot be detected [36, 42]. We want to emphasize and repeat at this point that these kinds of cell adhesion measurements are not limited to adhesion to the bare or protein-decorated quartz resonator but are also possible with a thin film of any material that can be precoated on the resonator as long as it fulfills the requirements mentioned earlier in the text.

We also studied the situation at the interface between surface and cell membrane by means of reflection interference contrast microscopy (RICM) that has been used extensively to image the footprints of cells on transparent substrates. In RICM, the cell-covered coverslip is illuminated from below and the reflected light is used for imaging. The light can either be reflected at the glass–medium interface or at the adjacent medium–membrane interface. Interference between the two provides a contrast that codes and maps the distance between membrane and

surface. In these experiments we seeded cells in serum-containing medium that was either supplemented with 1 mM RGDS (similar activity as GRGDS) or not. In both cases, the cells were allowed to attach and spread upon the glass surface for 200 min before we recorded RICM images of each sample. In the absence of RGDS the cells form typical cell–surface junctions with the substrate. The footprints indicate a spread morphology under these conditions. When RGDS is present the cells are hardly visible in the RICM image although they had settled on the surface. Based on the principles of RICM image formation and some experimental parameters of the microscope one can estimate that in the presence of 1 mM RGDS the lower cell membrane must be farther away from the substrate surface than 100 nm — probably significantly more — confirming the analysis of the QCM readings in the presence of these inhibitory peptides. Apparently, the presence of the cell bodies within this distance from the substrate surface and with only a very limited contact area — like a hard sphere on a flat surface — does not provide any significant acoustic load for the quartz resonator [17].

Thus, two main conclusions can be drawn from these experiments: (i) The QCM does only report on cells that are specifically anchored to the resonator surface. The method is blind to cells that just settle on the surface and attach only loosely. (ii) When specific cell–substrate interactions are absent, the cells stay away from the surface by more than 100 nm according to our RICM data. Theoretical considerations have previously indicated that cells may approach the surface as close as 5–10 nm just by unspecific attraction [47]. This is, however, neither confirmed by our optical measurements nor by the QCM data. We have already discussed above that the decay length of the mechanical oscillation in a QCM experiment in an aqueous environment at room temperature is approx. 250 nm. But apparently the loosely attached cell bodies (in presence of RGDS) are far enough away from the surface that the mechanical oscillation cannot sense them.

3.2.3. QCM Experiments with Well-Defined Model Systems

Due to the complex mechanical characteristics of living cells anchored to the resonator surface, which are inadequately described by the available micro-mechanical models, we studied chemically well-defined model systems to better understand what could be learned from QCM-based adhesion studies of animal cells [29, 48, 49]. As described for the ECIS experiments before, we used liposomes doped with varying amounts of biotinylated lipids to mimic the cell body (liposome) and its cell–surface receptors (biotin moieties). The adhesive proteins on the surface were modeled by a layer of pre-deposited avidin that provides binding sites for the biotin residues in the lipid shell. Thus, receptor density and protein concentration on the surface were under experimental control and could be adapted according to the experimental needs. In our initial studies we used large unilamellar vesicles made from dipalmitoylphosphatidylcholine (DPPC) doped with increasing molar ratios of dipalmitoylphosphatidylethanolamine (DPPE) carrying a biotin residue. The biotin was covalently attached to the lipid headgroup *via* a C_6 spacer.

In these experiments we used a special QCM setup that was originally described by Rodahl and coworkers [50] and is referred to as QCM-D. This device not only records the changes in resonance frequency Δf but also changes in the so-called dissipation factor D which is the inverse of the quality factor Q of the oscillation:

$$D = \frac{1}{Q} = \frac{\textit{Dissipated energy per cycle}}{\textit{Stored energy per cycle}}. \tag{6}$$

As expressed in equation (6), shifts in D reflect changes in energy dissipation of the shear oscillation. For dissipative systems the energy of the shear oscillation is transmitted into the material layer adsorbed on the quartz. Thus, measuring the change in energy dissipation becomes important whenever systems are studied that do not behave like a rigid mass. Only for homogeneous rigid mass films an experimentally observed frequency shift can be attributed unequivocally to mass deposition on the resonator surface according to the Sauerbrey relationship [33]. When the microviscosity or elasticity close to the quartz surface changes, the Sauerbrey equation no longer holds since these effects change the resonance frequency as well and are indistinguishable from simple mass deposition. Thus, viscous energy losses can make QCM measurements ambiguous and hard to interpret [51]. The device developed by Rodahl and coworkers [50] overcomes this problem by recording both the shift in resonance frequency as well as energy dissipation at the same time which makes data interpretation more robust and provides twice the information on the system under study.

When living animal cells were studied with this setup we typically found frequency shifts Δf between 50 and 500 Hz depending on the cell type. The cell-type specific change in dissipation factor ΔD ranged between 1 and 4×10^{-4} [48]. When we used undoped DPPC liposomes of 100 nm diameter that were allowed to settle on an avidin-coated resonator, we recorded frequency shifts in the order of 400–500 Hz, thus very similar to the readout for living cells even though these liposomes did not form specific molecular interactions with the surface-immobilized avidin. With respect to energy dissipation the liposomes, however, did not dissipate the same amount of energy as living cells did. For the undoped DPPC liposomes we observed an increase in energy dissipation in the order of 3×10^{-5} which is roughly an order of magnitude less than recorded for the substrate-anchored cells.

Adding biotin-labeled lipids in the liposome shell in order to allow for molecular recognition between liposome and surface bound protein led to a gradual reduction of both Δf and ΔD. As demonstrated in Fig. 12 there is a gradual drop in both parameters with increasing concentrations of biotin residues in the liposome shell. In other words, the more the ligand–receptor pairs were available the more the QCM response was reduced [48]. And this result does not depend on the size of the liposome. The data in figure 12 were recorded for large unilamellar liposomes with an average diameter of 100 nm but giant liposomes with diameters in the μm-range also showed a similar behavior. Even for these vesicles, that have roughly the size of a typical animal cell, we could not observe a similar energy dissipation as observed

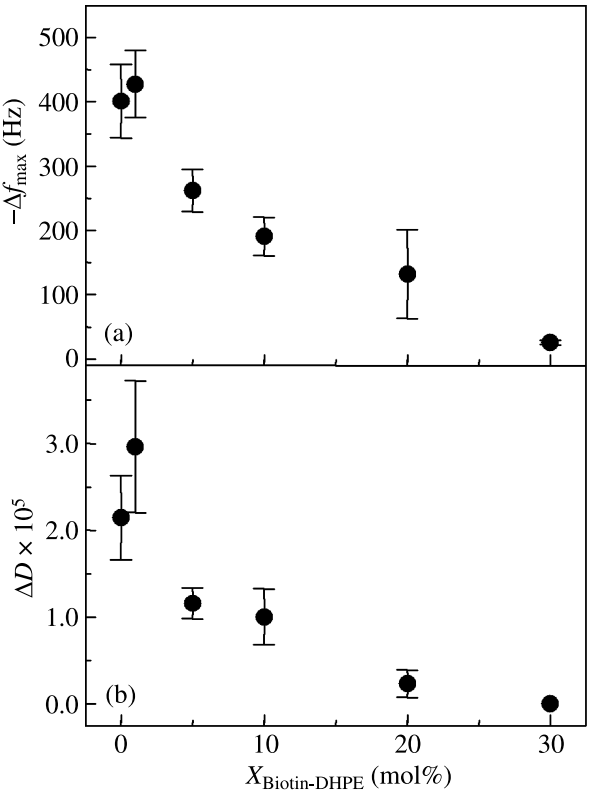

Figure 12. Summary of liposome adhesion studies as performed with a QCM-D setup described in the text. Panel (a) shows the maximum frequency shift Δf_{max} when the concentration of biotinylated lipids was gradually increased. Panel (b) summarizes the final shifts of the dissipation factor ΔD from the same experiments. Data points are averages of at least two independent experiments [48].

for adherent cells — independent of the presence or absence of specific molecular interactions.

The reason for this very unexpected behavior was revealed by scanning force microscopy [29]. With increasing biotin load in the liposome shell, the liposomes spread out on the surface. But eventually they rupture when the adhesion forces provided by the ligand–receptor interactions dominate over the intermolecular forces that keep the lipids together within the liposome shell. The ruptured liposomes eventually form a lipid double layer on the surface with the water-filled interior of the original liposome being emptied into the bulk phase. These lipid bilayers on the surface behave essentially like a rigid mass deposited on the surface so that the shifts in resonance frequency and dissipation decline. Kasemo and coworkers investigated this effect with similar model systems [52].

As a conclusion of this section, these experiments clearly revealed that unilamellar liposomes, as used here, are not a suitable model system to perform systematic studies of cell adhesion to *in vitro* surfaces by QCM — mostly due to the un-

avoidable rupture of the liposomes when surface attraction becomes too strong. Nevertheless, for intermediate biotin concentrations these experiments did show that an aqueous compartment surrounded by a lipid double layer was not sufficient to explain the high acoustic load that was exerted on the resonator by a confluent cell layer. There is more to it than just a membrane-confined fluid compartment close to the surface. As indicated several times throughout the last sections we have collected compelling evidence that the surface-facing membrane together with the cortical cytoskeleton and their micro-mechanical properties dominate the QCM readout. In other words, QCM-based adhesion studies provide a label-free and time-resolved view on the micromechanical changes at the substrate-facing lower membrane in addition to the time course of adhesion.

Acknowledgement

The authors would like to acknowledge generous financial support by the Kurt-Eberhard Bode Stiftung.

References

1. K. C. Dee, D. A. Puleo and R. Bizios, *Biocompatibility*. John Wiley & Sons, Chichester (2003).
2. P. Zilla, M. Deutsch and J. Meinhart, *Seminars Vascular Surg.* **12**, 52 (1999).
3. J. G. Meinhart, J. C. Schense, H. Schima, M. Gorlitzer, J. A. Hubbell, M. Deutsch and P. Zilla, *Tissue Eng.* **11**, 887 (2005).
4. T. Stieglitz, M. Schuettler and K. P. Koch, *IEEE Eng. Med. Biol. Mag.* **24**, 58 (2005).
5. P. Fromherz, *ChemPhysChem* **3**, 276 (2002).
6. T. Henning, M. Brischwein, W. Baumann, R. Ehret, I. Freund, R. Kammerer, M. Lehmann, A. Schwinde and B. Wolf, *Anticancer Drugs* **12**, 21 (2001).
7. I. Freshney, *Culture of Animal Cells: A Manual of Basic Techniques*. John Wiley & Sons, Chichester (2000).
8. T. Noll, N. Jelinek, S. Schmidt, M. Biselli and C. Wandrey, in: *Advances in Biochemical Engineering/Biotechnology*, T. Scheper (Ed.) **74**, p. 111. Springer Verlag (2002).
9. K. L. Prime and G. M. Whitesides, *Science* **252**, 1164 (1991).
10. M. Arnold, E. A. Cavalcanti-Adam, R. Glass, J. Blummel, W. Eck, M. Kantlehner, H. Kessler and J. P. Spatz, *ChemPhysChem* **5**, 383 (2004).
11. A. Pierres, A. M. Benoliel and P. Bongrand, *Eur. Cells Mater.* **3**, 31 (2002).
12. T. Frisch and O. Thoumine, *J. Biomech.* **35**, 1137 (2002).
13. A. S. G. Curtis, *Eur. Cells Mater.* **1**, 59 (2001).
14. Y. Iwanaga, D. Braun and P. Fromherz, *Eur. Biophys. J.* **30**, 17 (2001).
15. D. Braun and P. Fromherz, *Biophys. J.* **87**, 1351 (2004).
16. V. Kiessling, B. Müller and P. Fromherz, *Langmuir* **16**, 3517 (2000).
17. J. Wegener, in: *Encyclopedia of Biomedical Engineering*, M. Akay (Ed.) **6**, p. 1. Wiley & Sons, Hoboken, NJ (2006).
18. I. Giaever and C. R. Keese, *Nature* **366**, 591 (1993).
19. I. Giaever and C. R. Keese, *Proc. Natl Acad. Sci. USA* **81**, 3761 (1984).
20. R. Ehret, W. Baumann, M. Brischwein, A. Schwinde and B. Wolf, *Med. Biol. Eng. Comput.* **36**, 365 (1998).

21. L. Ceriotti, J. Ponti, P. Colpo, E. Sabbioni and F. Rossi, *Biosens. Bioelectron.* **22**, 3057 (2007).
22. D. Krinke, H. G. Jahnke, O. Panke and A. A. Robitzki, *Biosens. Bioelectron.* **24**, 2798 (2009).
23. I. Giaever and C. R. Keese, *Proc. Natl Acad. Sci. USA* **88**, 7896 (1991).
24. J. Wegener, in: *Nanotechnology*, H. Fuchs (Ed.) **6**, p. 325. VCH, Weinheim (2009).
25. J. Wegener, C. R. Keese and I. Giaever, *Exp. Cell. Res.* **259**, 158 (2000).
26. P. J. Salas, D. E. Vega-Salas and E. Rodriguez-Boulan, *J. Membr. Biol.* **98**, 223 (1987).
27. D. Kirchhofer, J. Grzesiak and M. D. Pierschbacher, *J. Biol. Chem.* **266**, 4471 (1991).
28. A. Sapper, B. Reiss, A. Janshoff and J. Wegener, *Langmuir* **22**, 676 (2006).
29. B. Pignataro, C. Steinem, H. J. Galla, H. Fuchs and A. Janshoff, *Biophys. J.* **78**, 487 (2000).
30. A. Janshoff and C. Steinem (Eds), *Piezoelectric Sensors*. Springer, Berlin (2007).
31. A. Janshoff, H.-J. Galla and C. Steinem, *Angew. Chemie Intern. Edition* **39**, 4004 (2000).
32. J. Wegener, A. Janshoff and C. Steinem, *Cell Biochem. Biophys.* **34**, 121 (2001).
33. G. Sauerbrey, *Z. Phys.* **155**, 206 (1959).
34. D. M. Gryte, M. D. Ward and W. S. Hu, *Biotechnol. Prog.* **9**, 105 (1993).
35. J. Redepenning, T. K. Schlesinger, E. J. Mechalke, D. A. Puleo and R. Bizios, *Anal. Chem.* **65**, 3378 (1993).
36. J. Wegener, A. Janshoff and H. J. Galla, *Eur. Biophys. J.* **28**, 26 (1998).
37. J. Wegener, S. Zink, P. Rosen and H. Galla, *Pflugers. Arch.* **437**, 925 (1999).
38. F. Josse, Y. Lee, S. J. Martin and R. W. Cernosek, *Anal. Chem.* **70**, 237 (1998).
39. A. Janshoff, J. Wegener, M. Sieber and H. J. Galla, *Eur. Biophys. J.* **25**, 93 (1996).
40. C. M. Marxer, M. C. Coen, T. Greber, U. F. Greber and L. Schlapbach, *Anal. Bioanal. Chem.* **377**, 578 (2003).
41. V. Heitmann, B. Reiss and J. Wegener, in: *Piezoelectric Sensors*, A. Janshoff and C. Steinem (Eds) **5**, p. 303. Springer, Berlin (2007).
42. J. Wegener, J. Seebach, A. Janshoff and H. J. Galla, *Biophys. J.* **78**, 2821 (2000).
43. M. Rodahl, F. Hook, C. Fredriksson, C. A. Keller, A. Krozer, P. Brzezinski, M. Voinova and B. Kasemo, *Faraday Discuss.* **107**, 229 (1997).
44. A. S. Cans, F. Hook, O. Shupliakov, A. G. Ewing, P. S. Eriksson, L. Brodin and O. Orwar, *Anal. Chem.* **73**, 5805 (2001).
45. P. Bongrand, *J. Dispersion. Sci. Technol.* **19**, 963 (1998).
46. G. I. Bell, M. Dembo and P. Bongrand, *Biophys. J.* **45**, 1051 (1984).
47. E. A. Vogler and Bussian, *J. Biomed. Mater. Res.* **21**, 1197 (1987).
48. B. Reiss, A. Janshoff, C. Steinem, J. Seebach and J. Wegener, *Langmuir* **19**, 1816 (2003).
49. E. Lüthgens, A. Herrig, K. Kastl, C. Steinem, B. Reiss, J. Wegener, B. Pignataro and A. Janshoff, *Measurement. Sci. Technol.* **14**, 1865 (2003).
50. M. Rodahl, F. Höök, A. Krozer, P. Brzezinski and B. Kasemo, *Rev. Sci. Instrum.* **66**, 3924 (1995).
51. M. V. Voinova, M. Jonson and B. Kasemo, *Biosens. Bioelectron.* **17**, 835 (2002).
52. E. Reimhult, M. Zach, F. Hook and B. Kasemo, *Langmuir* **22**, 3313 (2006).